FEM Study of Induction Machines Suffering from Rotor Electrical Faults Using Stray Flux Signature Analysis

Panagiotou, P., Arvanitakis, I., Lophitis, N. & Gyftakis, K. N

DOI 10.1109/ICELMACH.2018.8506707

Publisher: IEEE

FEM Study of Induction Machines Suffering from Rotor Electrical Faults Using Stray Flux Signature Analysis

P.A. Panagiotou, I. Arvanitakis, N. Lophitis, and K.N. Gyftakis

***Abstract*—The wide range of applications using induction machines has been enhanced with the rapid evolution of condition monitoring and variable speed drives. The latter two, along with their constantly growing demands, have raised the necessity of new approaches and techniques in fault diagnostics. A reliable solution to this matter, has proven to be the monitoring of stray magnetic flux. Accounted for in different locations on the machine's peripheral area and with different measurement techniques, the stray flux provides valuable information for fault detection and identification. This paper aims to apply one of these diagnostic strategies and the related measurement of stray flux using FEM, to evaluate its performance and diagnostic capability on two machines of different size and power rating and conclude on the quantitative effectiveness of such strategies.**

Keywords*—*stray flux, condition monitoring, induction machines, flux sensors.

I. Introduction

Three-phase induction motors are widely used in industrial and mobility applications. For both cases, heavy duty tasks with variable load conditions oblige the reliable monitoring of these motors, especially after long-term use [1]. Numerous approaches of condition monitoring techniques are found in the literature for fault detection and diagnostics in induction machines, namely: signal based methods, model based, circuit theory based and simulation based methods (*Finite Element Methods* - FEM) [1], [2]. Amongst them, signal-based Motor Current, or Voltage, Signature Analysis (MCSA and MVSA) -usually combined with FEM- are the most commonly known and, so far, mainly applied in the field. A representative background on these techniques is given in [1], [2] and [3].

Although MCSA has rendered valuable results for various types of faults, authors have often reported drawbacks of this method [3]–[8]. Hence, a trend for condition monitoring of induction machines using analysis of stray flux signals began in the late '80s [4]. This was followed by works of researchers who contributed to understanding and modelling the mechanisms that allow potent diagnostics based on stray flux measurements [6], [7]. Based upon the fact that no machine is ideal or perfectly manufactured and balanced, and -consequently- quantities of magnetic flux will stray in paths without being taken advantage of, this technique proposes capturing amounts of stray flux radiated on the external machine parts, like the machine's end windings or outside its frame [7], [8]. Due to the induction phenomena from the stator to the rotor and vice-versa, these portions of radiated stray flux are considered to enclose consolidated information about both stator and rotor quantities, in terms of time and space dependent harmonics [8]. These harmonics can be detected and studied through signals of voltage induced on search coils, located as close as possible to the end parts of the machine's periphery (stator end windings and rotor end rings). The analytical models for these harmonics have been formulated and provided not only theoretically, but have also been verified experimentally for machines under healthy and faulty operation [5], [7]–[9]. A simplified spectrum method for short circuits detection is given in [5], by inspection of signatures in the spectrum of induced voltage on a search coil coaxially placed with the shaft. The same authors successfully use this technique in [9] for different induction machines under variable load conditions to detect broken rotor bars, proving the method's increased sensitivity and reliability compared to conventional MCSA when the diagnostics deal with these types of motors.

Additionally, in [10] and [11] a multivariable monitoring method is introduced where the authors use vibration, currents and stray flux signal analysis to ensure diagnostic robustness and reliability for rotor defects under different load conditions. In [12], the potential of this alternative diagnostic method is again verified experimentally for inter-turn short circuits, while the same authors in [13] use a time-frequency representation to prove the method efficient for rotor fault detection after supply disconnection. Also, an intensive analysis of stray flux is given in [14] for monitoring an induction machine operating under gearbox coupling within an electromechanical system, where also the effects of the gearbox frequencies on torque oscillations are studied.

Several works have approached this matter with invasive monitoring, to capture the stray flux induced voltage using an internal search coil aiming to detect stator winding [15] or rotor fault conditions [16]. However, although the results are encouraging, invasive methods demand disassembling the rotor from the stator and recoiling the sensor along the stator core length. Furthermore, successful detection of dynamic and mixed eccentricity faults has been reported by stray flux signature analysis using Hall probes [17]. A Hall-effect sensor is also used in [18] for invasive monitoring of broken rotor bars.

An important contribution to the foundations of stray flux

Panagiotis A. Panagiotou is with School of Computing, Electronics and Mathematics, and Research Institute Future Transport & Cities, Coventry University, UK (e-mail: panagio4@uni.coventry.ac.uk).

Ioannis Arvanitakis is with School of Computing, Electronics and Mathematics, Coventry University, UK (e-mail: ac7632@coventry.ac.uk).

Neophytos Lophitis is with the Research Institute Future Transport & Cities and the School of Computing, Electronics and Mathematics, Coventry University, UK (e-mail: n.lophitis@coventry.ac.uk).

Konstantinos N. Gyftakis is with the Research Institute Future Transport & Cities and School of Computing, Electronics and Mathematics, Coventry University, UK (e-mail: k.n.gyftakis@ieee.org).

analysis is also provided in [19] and [20] for diagnosing rotor faults and stator faults respectively. The main added value of the latter two works does not only consist in the successful diagnostic procedure, but also in the examination of how the stray flux measurements are affected with regards to the flux sensor location and alignment on the machine periphery. This leads the authors to assess and categorize the stray flux signatures according to their origin from axial or radial attenuated stray flux.

In addition, in [21] the authors developed a stray flux measurement system using a "C" magnetic core flux sensor for assessing the measurements in three different locations outside the machine frame. Continuing this work concept-wise, in [22], they enhanced this system for detection of stator winding short circuits, while in [23] a comparison between axial and radial stray flux is addressed by means of statistical processing for the integer harmonics.

Thorough research on external magnetic field analysis, has also been applied for stray flux on the machine end-regions using 3-D FEM and stray losses analysis [24], a growler and magnetic viewing films for disassembled rotors [25] and Hall probes for air-gap eccentricity [26]. In [27], a covariance analysis is also delivered for the space and time harmonics of the stray flux, while [28] provides an insight to harmonics discrimination for both stator and rotor faults validated experimentally.

Following ongoing research developments of the last decade, sophisticated signal processing techniques like the Short-Time Fourier Transform and Wavelet Decomposition have been proposed for diagnosis through the stray flux fields during the start-up transient [29], [30]. These approaches are valuable for two reasons: first and foremost, they hold the potential for fast diagnosis during the machine start-up with the use of fault indicators, and, on the other hand, they also examine the differences of the method and the signatures' footprints with regards to the flux sensor position and the signals captured in each position. The latter is the most important, since the optimal number of sensors and their position or geometry for accurate and reliable signal acquisition is still being investigated. Innovative approaches of intelligent techniques for predictive vector control using magnetic field analysis under faulty operation have been attempted as well, for developing fault-tolerant control models [31]. Another study of rotor faults detection with spectrum-based analysis of radial flux is given in [32] using a Fluxgate sensor, the position of which is examined later in [33] under different load torque profiles. Finally, one of the latest reviews on how stray flux based monitoring techniques are applied for cases of various types of faults, is given in [34].

In this paper, two different induction motors are investigated under stray flux signature analysis (SFSA). For this work, an industrial $1.1\ MW$ ($1475\ hp$) and a small $4\ kW$ ($5.4\ hp$) induction motor, are simulated with 2-D FEM and are analyzed under healthy condition, as well as under the broken bar faults. The stray flux signals are captured with a search coil placed externally from the machine's housing. The study aims to recognize the fault signatures and their behavioral differences in the frequency spectrum for a comparison between small and large machines under healthy operation and the broken bar condition.

The paper is structured as follows: in Section II, a brief presentation of the theoretical background for existing stray flux methods is provided. Also, the difference between measurement of axial and radial stray flux and existing measurement acquisition techniques are outlined. In Section III the FEM models are described, followed by the results from FEM simulations presented and explained in Section IV for the two induction motors under investigation, leading to the conclusions in Section V.

II. Theoretical Background

A. Stray Flux Methods & Stray Flux Signature Analysis

Since every phenomenon that occurs in either the stator or the rotor is induced and filtered from one to another and so on, the stray flux is a signal in whose signatures, fault asymmetries will be reflected [5], [7]–[9]. In fact, considering that the stators construction and the surrounding housing resemble a magnetic shield effect, the stator quantities signatures are predominantly present [10]. However, the magnetic fields that are present in an induction machine are three: the main magnetizing field flowing from the stator teeth to the rotor teeth through the air-gap, the stator leakage field due to stator slot openings, stator frame and stator yoke and -finally- the rotor leakage field due to rotor slot openings, rotor yoke and rotor shaft [6], [21]–[23]. Hence, the stator quantities' signatures prevail, without though disallowing the presence of frequency components sensitive to asymmetries induced by the rotor. Such frequency components are detected around the frequencies f_s, $3f_s$, $5f_s$, as well as the low frequency component $f_s - f_r$, with f_s being the fundamental supply frequency, f_r the rotor rotational frequency and s the motor slip [9], [13], [19]. The formula for the stator-related frequencies under the broken bar fault is given by the following equation [3]:

$$f_{bb} = [\frac{k}{p}(1-s) \pm s]f_s \ , \tag{1}$$

where p is the number of pole pairs and $k/p \ \in \mathbb{Z}$.

Also, due to the aforementioned rotating leakage fields' distribution and pathways, the method of flux sensing accounts for different type of flux with regards to the position of the sensor, being: pure axial, pure radial or mixed radial/axial portions of stray flux. The last case would be the most convenient for a diagnostic process, but is not always possible to achieve, as will be explained in next Subsection II-B.

Being a quantity sensitive to noise though, the stray flux is mainly analyzed and studied in the low frequencies range [3], [5]–[11], [18]–[28]. This is not only because the low frequency components are easier to detect in SFSA, but also because the induced voltage on the sensor accrues from derivation of the actual flux and the derivation can affect the amplitudes of the high frequency components [10], [23], [27].

B. Stray Flux Measurements

Different measurement techniques have been applied by researchers who undertake investigation of diagnostics through stray flux monitoring. Since the stray flux attenuated on the vicinity of the motor is a quantity with complex 3-D geometrical pattern not easily obtained and modelled, the idea behind the coil measurement attempts and trials so far is to

embrace as much portion of flux as possible, in order to observe the behavior of harmonics and evaluate what changes these harmonics undergo in the spectra [22], [23], [25]–[28]. Thus, different types of sensors and various uses of those have been presented so far. The instruments dealt with in most of the works, are flux sensors consisting of air coils with several hundreds of turns. That is because they provide a low-cost solution with relatively easy application of the instrument around the motor. These can be placed in two positions: either frontal or lateral [29], [30].

In the frontal position, it will be either a search coil placed coaxially with the machine shaft -a part of the machinery which is not easily accessible when applying condition monitoring on the field- or a number of sensors placed in quartiles symmetrically from the machine shaft. This way, the induced voltage withholds information regarding axial stray flux only [19], [28]. This kind of measurement is preferred to be taken on the machine end parts (stator end-winding and rotor end rings), and therefore an alternative position for the sensor is the symmetrical one, meaning the machine fan side. In that case though, according to the application, appropriate signal filtering must be applied because the fan and cooling systems on this part of the machine are known to be sources of noise, which becomes excessive in industrial environments where series of motors are coupled or next to each other, i.e. production lines or power plants.

Another type of measurement that is encountered in the literature, is the measurement of pure radial flux. This can be done with search coils placed laterally and in parallel with the plane defined by the machine's traverse cross-section plane, and it can be either done close to the end parts or not [19], [20], [28]–[30], [34]. What is suggested for the instrument is that its length and diameter should be much less than the total machine height in order to capture satisfying amount of flux lines [8], [18], [21]–[23]. This is the type of stray flux condition handled in this paper.

Finally, in the lateral position, if the sensing coil is placed in a way that its girth lies on the machine precinct side and coincides with it, the measurement of mixed axial and radial flux is derived by the instrument [10], [12], [13], [22]. This is the most preferable case, since more signatures are captured to be studied, but the frequency components arising in the spectra have yet not been fully discriminated and categorized, apart from the low frequency range for rotor inherent asymmetries or a few cases of broken bars, as well as high order-harmonics for PSH and source supply harmonics. However, 2-D FEM cannot account for this type of stray flux, because it strictly requires a 3-D geometry.

III. FEM Models

For the purpose of the analysis, two different induction machines were modelled and simulated with "MagNet" FEM software, provided by Infolytica, under rotary load driven motion -accounting for the machine's motion equation and moment of inertia- from the start-up transient until the steady state. The FEM models take into account the exact geometrical and materials characteristics as provided from the manufacturers. The analysis is held under rated load condition for both motors and the load coupled directly to the shaft, accounting for them being in healthy operation and operations with their rotors suffering from one broken bar. In Fig. 1 the two models are shown along with the corresponding magnetic field distribution (magnetic flux density $\boldsymbol{B}$ $[Tesla]$), when the motors are in healthy mode.

TABLE I
Characteristics of the motors under study

Characteristics	Motor # 1	Motor # 2
Supply Frequency f_s	50 Hz	50 Hz
Stator Connection	$\triangle$	$\curlywedge$
Output Power	3 kW	1.1 MW
Rated Voltage	270 V	4.7 V
Rated Current	8.6 A	170 A
Number of Poles	4	6
Rated Speed	1416 rpm	990 rpm
Number of stator slots	36	54
Number of rotor bars	32	70

Fig. 1(a) depicts the first motor under examination, which is a small laboratory, or small scale mobility, oriented induction motor. Operating at 50 Hz, with nominal characteristics 400 V, 4 kW, this Δ-connected, 4-pole three-phase induction motor encloses a 32 bar aluminum die cast rotor inside a stator designed with 36 stator slots and a single layer 49-turn per slot winding.

Secondly, an industrial Y-connected, 6-pole, 6.6 kV, 1.1 MW, 50 Hz cage induction motor has been studied, with the rotor cage fabricated from 70 copper bars and the stator of 54 slots with a 12-turn per slot double layer 1 to 9 pitched winding. This motor is depicted in Fig. 1(b). A brief description of the modelled motors, is given in Table I.

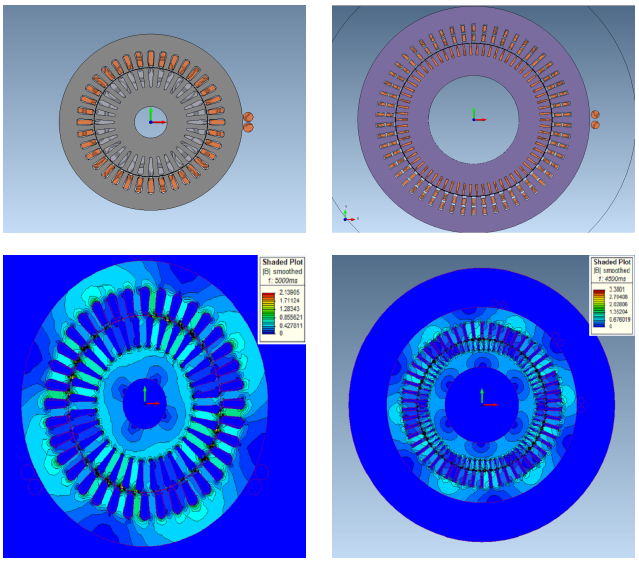

(a) (b)

Fig. 1: (a) Top: healthy $4kW$ machine, Bottom: corresponding magnetic field and (b) Top: healthy $1.1MW$ machine, Bottom: corresponding magnetic field

To aid the reader, the two distinct FEM cases of the 4 kW and 1.1 MW motors are labeled and referred to as "Motor #1" and "Motor #2" respectively. The motors under the broken bar fault and the corresponding magnetic flux density distribution are shown in Fig. 2.

The flux sensor is a stranded 100-turn search coil, with

the input and output wounded on a point of the machine's periphery close to the stator frame.

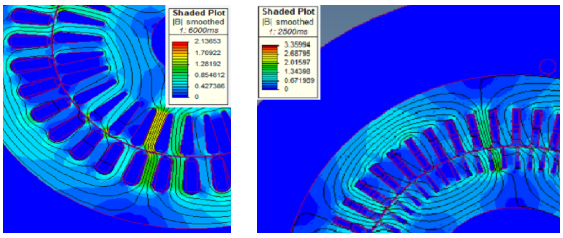

(a) (b)

Fig. 2: Magnetic Field Distributions for (a) Motor # 1 and (b) Motor # 2 under one broken rotor bar fault

For reliable signal representation in both time and frequency domain and improved spectral resolution, the total signal acquisition time with FEM was ≈7.5 seconds for each motor with a sampling frequency of 10 kHz. However, for the application of the FFT only the steady state of the signals is used, which is ≈6.5 seconds for Motor #1 and ≈4.5 seconds for Motor #2. The signals are downsampled with a factor of 2 and prefiltered for the FFT with a low pass filter at the cut-off frequency of 2 kHz.

IV. FEM Results on Stray Flux

For the spectral analysis, the FFT -over a Hann window to avoid spectral leakage- is applied to the signal of the voltage induced on the search coil. Focus will be given to the stray flux broken rotor bar fault sidebands given from (1), hence sidebands around the frequencies $f_s - f_r$, f_s, $3f_s$ and $5f_s$, where f_s the supply frequency (Hz).

Fig. 3 depicts the harmonic content of the stray flux in Motor #1, under healthy (blue) and faulty operation with one broken bar (red) and the spectrum has been normalized to 0 dB with respect to the fundamental harmonic. The presented sideband signatures are the ones around the $f_s - f_r$ harmonic (Fig. 3(a)), around the fundamental 50 Hz harmonic (Fig. 3(b)), then around the 3rd stray flux harmonic (Fig. 3(c)) and, finally, around the 5^{th} harmonic (Fig. 3(d)). The central main frequencies are pointed in each spectrum with a red arrow, while the sidebands under examination with black ones.

In Fig. 4, the spectra of stray flux is given for the industrial 1.1 MW induction motor (Motor #2) at the same frequency areas as for Motor #1. In Table II, a comparison between the amplitudes of the radial stray flux harmonics is given for Motor #1 under healthy and faulty condition. Respectively, Table III provides the same comparison for the harmonics of Motor #2. The rotor mechanical frequency f_r is calculated for each motor by the formula:

$$f_r = \frac{(1-s)f_s}{p} \ , \tag{2}$$

where: s is the slip, p the pole pairs and f_s the supply frequency. In the last column of each table, the amplitude difference of each fault sideband signature from its central harmonic (pointed with red arrow in the spectra) is given.

Starting with the frequency of the $f_s - f_r$ for Motor #1 and comparing the amplitudes between healthy and faulty

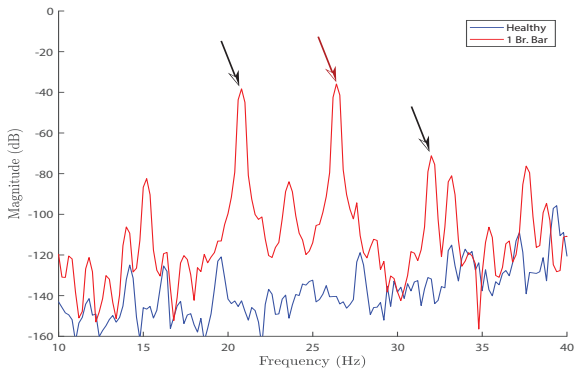

(a)

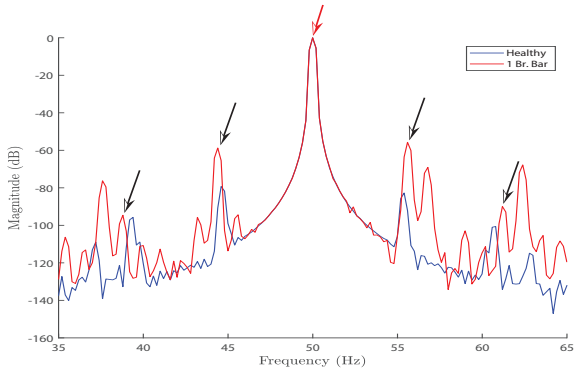

(b)

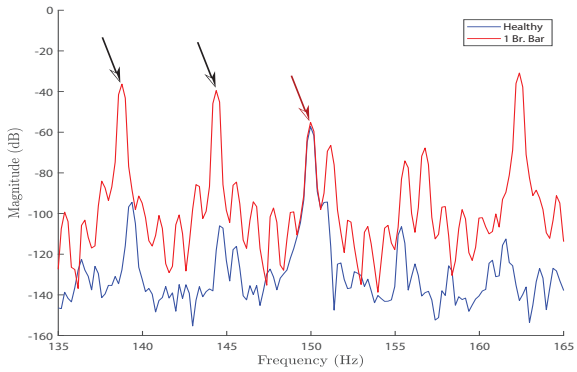

(c)

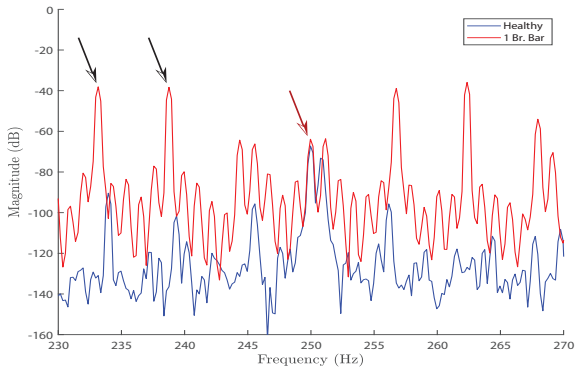

(d)

Fig. 3: FFT Spectra of the stray flux under healthy operation (blue) and one broken bar (red) for the $4kW$ motor at the frequency area of : (a)$f_s - f_r$, (b) f_s, (c) $3f_s$ and (d) $5f_s$.

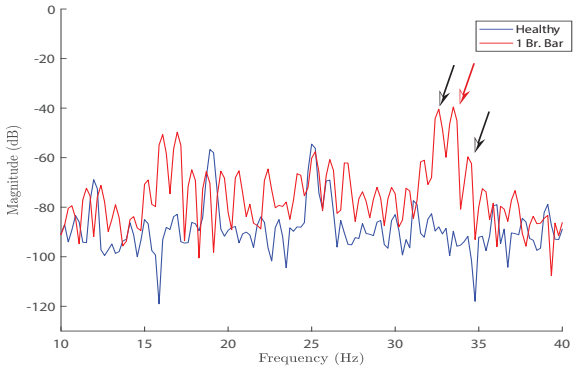

(a)

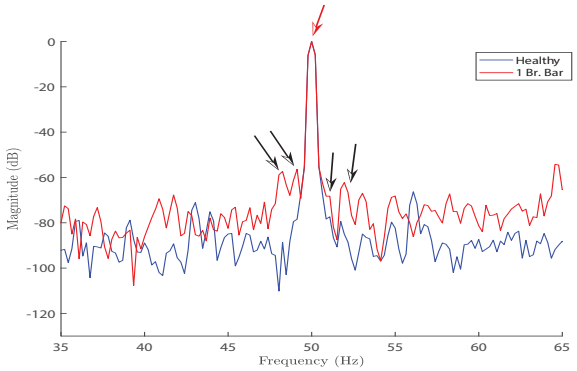

(b)

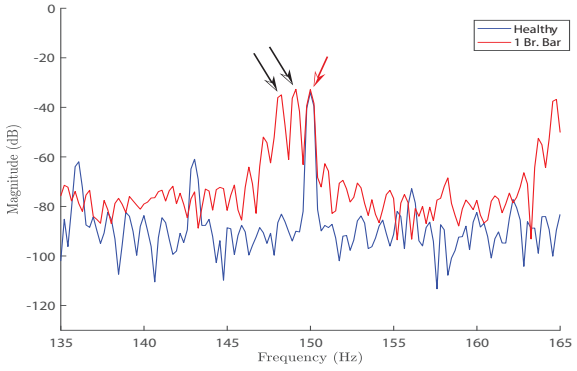

(c)

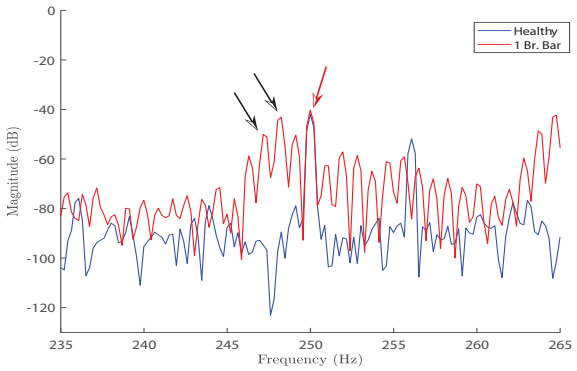

(d)

Fig. 4: FFT Spectra of the stray flux under healthy operation (blue) and one broken bar (red) for the $1.1MW$ motor at the frequency area of : (a)$f_s - f_r$, (b) f_s, (c) $3f_s$ and (d) $5f_s$.

TABLE II
Radial Flux Frequency Components & Amplitudes for Motor #1 under healthy Operation and 1 Broken Rotor Bar

Motor #1 - 5.4 hp, $\triangle$ Connected, 50 Hz, $p = 2$					
Frequency Component	**Healthy** ($s \approx 0.0534$)		**1 Broken Bar** ($s \approx 0.0562$)		**Difference**
	Hz	dB	Hz	dB	dB
$f_s - f_r$	26.33	-140.4	26.42	-35.98	-
$f_s - f_r - 2sf_s$	20.99	-142.5	20.74	-38.29	**2.31**
$f_s - f_r + 2sf_s$	31.68	-136.7	32.1	-71.21	**35.23**
$f_s - 2sf_s$	44.66	-79.32	44.38	-58.75	-
$f_s - 4sf_s$	39.32	-95.74	38.76	-94.59	-
$f_s + 2sf_s$	55.34	-82.74	55.62	-55.73	-
$f_s + 4sf_s$	60.68	-100.6	61.24	-89.96	-
$3f_s$	150	-57.22	150	-55.12	-
$3f_s - 2sf_s$	144.6	-106	144.38	-39.51	**15.61**
$3f_s - 4sf_s$	139.32	-94.48	138.76	-36.31	**18.81**
$5f_s$	250	-67.18	250	-63.87	-
$5f_s - 4sf_s$	239.32	-101.6	238.76	-38.33	**25.54**
$5f_s - 6sf_s$	233.98	-90.41	233.14	-38.12	**25.75**

TABLE III
Radial Flux Frequency Components & Amplitudes for Motor #2 under healthy Operation and 1 Broken Rotor Bar

Motor #2 - 1475 hp, $\curlywedge$ Connected, 50 Hz, $p = 3$					
Frequency Component	**Healthy** ($s \approx 0.0091$)		**1 Broken Bar** ($s \approx 0.0092$)		**Difference**
	Hz	dB	Hz	dB	dB
$f_s - f_r$	33.48	-89.68	33.48	-39.52	-
$f_s - f_r - 2sf_s$	32.61	-87.93	32.61	-40.4	**0.88**
$f_s - f_r + 2sf_s$	34.35	-91.75	34.35	-59.67	**20.15**
$f_s - 2sf_s$	49.13	-78.44	49.1335	-56.37	-
$f_s - 4sf_s$	48.26	-88.69	48.26	-57.34	-
$f_s + 2sf_s$	50.87	-78.36	51.08	-68.25	-
$f_s + 4sf_s$	51.74	-79.37	51.95	-62.25	-
$3f_s$	150	-33.98	150	-32.83	-
$3f_s - 2sf_s$	149.1	-89.99	149.1	-32.71	**0.12**
$3f_s - 4sf_s$	148.3	-83.11	148.3	-34.97	**2.14**
$5f_s$	250	-41.914	250	-40.24	-
$5f_s - 4sf_s$	248.3	-89.46	248.35	-43.12	**2.88**
$5f_s - 6sf_s$	247.2	-94.78	247.2	-50.11	**9.87**

operation, it is observed from Table II and Fig. 3(a) that the amplitude of the central frequency exhibits an increase of $104.42\ dB$, while the left and right sideband fault related signatures present an increase of $104.21\ dB$ and $65.49\ dB$ respectively. As for Motor #2 under the broken bar fault, the central $f_s - f_r$ frequency increases $50.16\ dB$, the $-2sf_s$ sideband component $47.53\ dB$ and the right $+2sf_s$ signature increases $32.8\ dB$ with respect to the healthy model (Fig. 4(a) and Table III). Furthermore, the amplitude difference of the left and right sidebands from the central frequency of Motor #1 have the values of $2.31\ dB$ and $35.23\ dB$ respectively, which clearly shows that the $-2sf_s$ sideband undergoes the largest difference and its peak reaches close to the amplitude of the fundamental, as expected. Similarly, Motor #2 presents the same behavior, having the $-2sf_s$ signature close to the central frequency with an amplitude difference of $0.88\ dB$, and the $+2sf_s$ quite low, showing a difference of $20.15\ dB$ from the $f_s - f_r$ component.

Regarding the fundamental $50Hz$ frequency area of Motor #1 (Fig. 3(b)), the $-2sf_s$ fault signature lies at $-58.75\ dB$ (increases $20.57\ dB$ from healthy motor) and the $-4sf_s$ component lies at $-94.59\ dB$ (having increased $1.15\ dB$ with respect to the healthy motor). The same signatures around $50Hz$ for Motor #2 (Fig. 4(b)) find themselves at

$-56.37\ dB$ showing an increase of $22.07\ dB$ ($-2sf_s$), and at $-57.34\ dB$ ($-4sf_s$), and increase $31.35\ dB$ compared to the healthy mode. Focusing on the right sidebands of $+2sf_s$ and $+4sf_s$, which are caused by the speed ripple effect [35], these signatures are noticed to have an amplitude of $-55.73\ dB$ and $-89.96\ dB$ respectively for Motor #1. Using the motor's healthy mode as a baseline, this is an increase of $27.01\ dB$ and $10.64\ dB$ respectively. The speed ripple sidebands of Motor #2 find themselves at $-68.25\ dB$ ($+2sf_s$) and at $-62.25\ dB$ ($+4sf_s$), which means an increase of $10.11\ dB$ for the $+2sf_s$ sideband and $17.12\ dB$ for the $+4sf_s$ compared to the healthy model. This is interesting, since the speed ripple effect, which is weaker on the large motor due to the motor's higher rotor inertia, seems to affect more the small motor (Motor #1) than the large one (Motor #2), which is due to the high rotor moment of inertia of the large motor. As a result, the right fundamental sideband is more reliable in small machines rather in large ones. However the $+4sf_s$ signature appears to be more sensitive in the large motor.

Another interesting observation, which is addressed from Fig. 3(c) and Fig. 4(c), concerns the saturation related (3^{rd}) harmonic and its fault sideband signatures. As it is also shown in Table II, the $-2sf_s$ and $-4sf_s$ components of Motor #1 display a difference of $15.61\ dB$ and $18.81\ dB$ respectively from the 3^{rd} harmonic. However, for Motor #2 the 3^{rd} harmonic sideband at $-2sf_s$ presents a difference of $0.12\ dB$ and the $-4sf_s$ signature difference holds the value of $2.14\ dB$ from the 3^{rd} harmonic. This is interesting to notice, since the iron core saturation for Motor #2 is lower than the iron core saturation level of Motor #1, as also shown in Fig. 1 (bottom), where the magnetic field distributions are shown for both motors.

Finally, a similar behavior is noticed with regards to the 5^{th} harmonic and the corresponding sidebands. The $-4sf_s$ signature of Motor #1 shows a difference of $25.54\ dB$ from the $250Hz$ harmonic, while the sideband component $-6sf_s$ a $25.75\ dB$ difference. For Motor #2, though, these differences from the main $250Hz$ harmonic are at $2.88\ dB$ for the $-4sf_s$ sideband and $9.87\ dB$ for the sideband at $-6sf_s$. Similarly with the 3^{rd} harmonic, the sidebands of the 5^{th} are also indicative for the fault, since the small difference from the central harmonic is indicative that the sideband exhibits a larger increase than the corresponding sideband of Motor #1. From the results a conclusion is drawn, that the use of higher stray flux signatures for the detection of broken rotor bars is more reliable and the signatures more sensitive to the fault for the large machine.

V. Conclusion

In this work, two different induction motors of different power sizes, suffering from a broken rotor bar fault, have been studied under 2D-FEM using stray flux signature analysis. The broken bar fault signatures of the radial stray flux were examined for the 1^{st}, 3^{rd} and 5^{th} harmonics' sidebands, as well as the sidebands of the rotor mechanical speed related component $f_s - f_r$. Also, the difference of each sideband from its main central harmonic was given as an indication of the rise each sideband undergoes in amplitude.

The results indicate that the examination of the low frequency component $f_s - f_r$ and its $\pm 2sf_s$ and $\pm 4sf_s$ sidebands perform a similar behavior for both motors and the calculated differences of amplitudes' increase are relatively close, regardless the dB amplitudes. Also, it is reported that the speed ripple sideband at $f_s + 4sf_s$ affects more intense the large motor showing a lager increase and small difference from the central harmonic, although the speed ripple effect is weaker for a large motor and although the bar asymmetry is of lower analogy (1 bar out of 70 bars is broken compared to 1 out of 36 in the small motor).

Regarding the 3^{rd} harmonic of each motor, which is a saturation related harmonic, it is compelling that despite the fact that the large motor exhibits lower iron-core saturation level, the difference of the saturation harmonic sidebands can be more reliably indicative for a broken bar asymmetry. Similar behavior with the 3^{rd} harmonic sidebands was observed for the sideband signatures of the 5^{th} harmonic, with only difference that the first left sideband at $-4sf_s$ and its relative difference show better diagnostic potential than the $-6sf_s$.

Acknowledgment

The authors would like to acknowledge Coventry University Doctoral College and Centre for Global Engagement Office for the support.

References

[1] H. A. Toliyat, S. Nandi, S. Choi, and H. Meshgin-Kelk, *Electric machines: modeling, condition monitoring, and fault diagnosis*. CRC press, 2012.

[2] J.-C. Trigeassou, *Electrical Machines Diagnosis*. John Wiley & Sons, Inc, 2013.

[3] J. Milimonfared, H. M. Kelk, S. Nandi, A. Minassians, and H. A. Toliyat, "A novel approach for broken-rotor-bar detection in cage induction motors," *IEEE Transactions on Industry Applications*, vol. 35, no. 5, pp. 1000–1006, 1999.

[4] J. Penman, H. G. Sedding, B. A. Lloyd, and W. T. Fink, "Detection and location of interturn short circuits in the stator windings of operating motors," *IEEE Transactions on Energy Conversion*, vol. 9, no. 4, pp. 652–658, Dec 1994.

[5] T. Assaf, H. Henao, and G. A. Capolino, "Simplified axial flux spectrum method to detect incipient stator inter-turn short-circuits in induction machine," in *IEEE International Symposium on Industrial Electronics*, vol. 2, May 2004, pp. 815–819 vol. 2.

[6] H. Meshgin-Kelk, J. Milimonfared, and H. A. Toliyat, "Interbar currents and axial fluxes in healthy and faulty induction motors," *IEEE Transactions on Industry Applications*, vol. 40, no. 1, pp. 128–134, 2004.

[7] H. Henao, G. A. Capolino, and C. Martis, "On the stray flux analysis for the detection of the three-phase induction machine faults," in *38th IAS Annual Meeting on Conference Record of the Industry Applications Conference*, vol. 2, Oct 2003, pp. 1368–1373.

[8] H. Henao, C. Demian, and G. A. Capolino, "A frequency-domain detection of stator winding faults in induction machines using an external flux sensor," *IEEE Transactions on Industry Applications*, vol. 39, no. 5, pp. 1272–1279, Sept 2003.

[9] A. Yazidi, H. Henao, and G.-A. Capolino, "Broken rotor bars fault detection in squirrel cage induction machines," in *Electric Machines and Drives, 2005 IEEE International Conference on*. IEEE, 2005, pp. 741–747.

[10] A. Bellini, C. Concari, G. Franceschini, C. Tassoni, and A. Toscani, "Vibrations, currents and stray flux signals to asses induction motors rotor conditions," in *IECON 2006 - 32nd Annual Conference on IEEE Industrial Electronics*, Nov 2006, pp. 4963–4968.

[11] C. Concari, G. Franceschini, and C. Tassoni, "Differential diagnosis based on multivariable monitoring to assess induction machine rotor conditions," *IEEE Transactions on Industrial Electronics*, vol. 55, no. 12, pp. 4156–4166, 2008.

[12] A. Yazidi, H. Henao, G. Capolino, M. Artioli, F. Filippetti, and D. Casadei, "Flux signature analysis: An alternative method for the fault diagnosis of induction machines," in *IEEE Russia Power Tech*. IEEE, 2005, pp. 1–6.

[13] S. H. Kia, H. Henao, G.-A. Capolino, and C. Martis, "Induction machine broken bars fault detection using stray flux after supply disconnection," in *32nd Annual Conference on Industrial Electronics*. IEEE, 2006, pp. 1498–1503.

[14] S. R. Fatemi, H. Henao, and G. Capolino, "Gearbox monitoring by using the stray flux in an induction machine based electromechanical system," in *The 14th IEEE Mediterranean Electrotechnical Conference, MELECON*. IEEE, 2008, pp. 484–489.

[15] P. Lamim Filho, R. Pederiva, and J. Brito, "Detection of stator winding faults in induction machines using flux and vibration analysis," *Mechanical Systems and Signal Processing*, vol. 42, no. 1-2, pp. 377–387, 2014.

[16] M. F. Cabanas, F. Pedrayes, M. G. Melero, C. H. R. Garcia, J. M. Cano, G. A. Orcajo, and J. G. Norniella, "Unambiguous detection of broken bars in asynchronous motors by means of a flux measurement-based procedure," *IEEE Transactions on Instrumentation and Measurement*, vol. 60, no. 3, pp. 891–899, 2011.

[17] O. Vitek, M. Janda, V. Hajek, and P. Bauer, "Detection of eccentricity and bearings fault using stray flux monitoring," in *Diagnostics for Electric Machines, Power Electronics & Drives (SDEMPED), 2011 IEEE International Symposium on*. IEEE, 2011, pp. 456–461.

[18] C. G. Dias and I. E. Chabu, "Spectral analysis using a hall effect sensor for diagnosing broken bars in large induction motors," *IEEE Transactions on Instrumentation and Measurement*, vol. 63, no. 12, pp. 2890–2902, 2014.

[19] A. Ceban, R. Pusca, and R. Romary, "Study of rotor faults in induction motors using external magnetic field analysis," *IEEE Transactions on Industrial Electronics*, vol. 59, no. 5, pp. 2082–2093, 2012.

[20] R. Romary, R. Pusca, J. Lecointe, and J. Brudny, "Electrical machines fault diagnosis by stray flux analysis," in *IEEE Workshop on Electrical Machines Design Control and Diagnosis (WEMDCD)*. IEEE, 2013, pp. 247–256.

[21] L. Frosini, A. Borin, L. Girometta, and G. Venchi, "Development of a leakage flux measurement system for condition monitoring of electrical drives," in *IEEE International Symposium on Diagnostics for Electric Machines, Power Electronics & Drives (SDEMPED)*. IEEE, 2011, pp. 356–363.

[22] L. Frosini, A. Borin, L. Girometta, and G. Venchi, "A novel approach to detect short circuits in low voltage induction motor by stray flux measurement," in *XXth International Conference on Electrical Machines (ICEM)*. IEEE, 2012, pp. 1538–1544.

[23] L. Frosini, C. Harlişca, and L. Szabó, "Induction machine bearing fault detection by means of statistical processing of the stray flux measurement," *IEEE Transactions on Industrial Electronics*, vol. 62, no. 3, pp. 1846–1854, 2015.

[24] J. Cheaytani, A. Benabou, A. Tounzi, M. Dessoude, L. Chevallier, and T. Henneron, "End-region leakage fluxes and losses analysis of cage induction motors using 3-d finite-element method," *IEEE Transactions on Magnetics*, vol. 51, no. 3, pp. 1–4, 2015.

[25] S. W. Clark and D. Stevens, "Induction motor rotor bar damage evaluation with magnetic field analysis," *IEEE Transactions on Industry Applications*, vol. 52, no. 2, pp. 1469–1476, 2016.

[26] I. Chernyavska and O. Vítek, "Analysis of air-gap eccentricity in inverter fed induction motor by means of motor current signature analysis and stray flux of motor," in *11th International Symposium on Diagnostics for Electrical Machines, Power Electronics and Drives (SDEMPED)*. IEEE, 2017, pp. 72–76.

[27] G. Mirzaeva, K. I. Saad, and M. G. Jahromi, "Comprehensive diagnostics of induction motor faults based on measurement of space and time dependencies of air gap flux," *IEEE Transactions on Industry Applications*, vol. 53, no. 3, pp. 2657–2666, 2017.

[28] P. Ewert, "Use of axial flux in the detection of electrical faults in induction motors," in *International Symposium on Electrical Machines (SME)*. IEEE, 2017, pp. 1–6.

[29] J. Antonino-Daviu, A. Quijano-López, V. Climente-Alarcon, and H. Razik, "Evaluation of the detectability of rotor faults and eccentricities in induction motors via transient analysis of the stray flux," in *IEEE Energy Conversion Congress and Exposition (ECCE)*. IEEE, 2017, pp. 3559–3564.

[30] J. Antonino-Daviu, H. Razik, A. Quijano-Lopez, and V. Climente-Alarcon, "Detection of rotor faults via transient analysis of the external magnetic field," in *43rd Annual Conference of the IEEE Industrial Electronics Society (IECON)*, Oct 2017, pp. 3815–3821.

[31] E. Ghosh, A. Mollaeian, S. Kim, J. Tjong, and N. C. Kar, "Intelligent flux predictive control through online stator inter-turn fault detection for fault-tolerant control of induction motor," in *2017 IEEE International Conference on Industrial Technology (ICIT)*. IEEE, 2017, pp. 306–311.

[32] T. Goktas, M. Arkan, M. S. Mamis, and B. Akin, "Broken rotor bar fault monitoring based on fluxgate sensor measurement of leakage flux," in *IEEE International Electric Machines and Drives Conference (IEMDC) 2017*. IEEE, 2017, pp. 1–6.

[33] L. Flux, T. Goktas, M. Arkan, M. S. Mamis, and B. Akin, "Separation of induction motor rotor faults and low frequency load oscillations through the radial," in *IEEE Energy Conversion Congress and Exposition (ECCE)*. IEEE, 2017, pp. 3165–3170.

[34] C. Jiang, S. Li, and T. G. Habetler, "A review of condition monitoring of induction motors based on stray flux," in *Energy Conversion Congress and Exposition (ECCE), 2017 IEEE*. IEEE, 2017, pp. 5424–5430.

[35] F. Filippetti, G. Franceschini, C. Tassoni, and P. Vas, "Ai techniques in induction machines diagnosis including the speed ripple effect," *IEEE Transactions on Industry Applications*, vol. 34, no. 1, pp. 98–108, 1998.

BIOGRAPHIES

Panagiotis A. Panagiotou was born in Thessaloniki, Greece, in June 1989. He received the 5 year Diploma in Electrical and Computer Engineering from the University of Patras, Greece, in 2015 and the MSc in Complex Systems & Network Theory from Aristotle University of Thessaloniki, Department of Mathematics, Greece, in 2017. Currently, he is a Ph.D Candidate with the Research Institute Future Transport & Cities and Coventry University, UK. His research is focused on condition monitoring and fault diagnosis of electric motors for industrial and EV applications, as well as statistical modelling and signal processing for diagnostic purposes.

Ioannis Arvanitakis received his 5 year Diploma in Electrical & Computer Engineering from University of Patras, Greece in 2009, and his Ph.D. from the same institution in 2017, entitled "Navigation and Collaborative Mapping of a Team of Mobile Robots". He is currently an Assistant Lecturer in Electrical and Electronics, School of Computing, Electronics and Mathematics, Coventry University, UK. His main research interests include, Navigation, Guidance and Control, Obstacle Avoidance algorithms, Unmanned Ground Vehicles, Simultaneous Localization and Mapping (SLAM) algorithms, Nonlinear Modeling, Optimization Theory.

Neophytos Lophitis is currently a Lecturer of Electrical Engineering at the School of Computing, Electronics and Mathematics and an associate with the Faculty Research Institute Future Transport & Cities within the Faculty of Engineering, Environment and Computing, Coventry University. He is also an Academic Collaborator with the High Voltage Microelectronics laboratory within the Department of Engineering, Electrical Division, of the University of Cambridge. He received the B.A. and M.Eng degrees in 2009 and the Ph.D degree in 2014, all from the University of Cambridge. His research activities are in optimization, design, degradation and reliability of high voltage microelectronic devices and electrical energy storage and conversion systems.

Konstantinos N. Gyftakis was born in Patras, Greece, in May 1984. He received the Diploma in Electrical and Computer Engineering from the University of Patras, Greece in 2010. He pursued a Ph.D in the same institution in the area of electrical machines condition monitoring and fault diagnosis (2010-2014). Then he worked as a Post-Doctoral Research Assistant in the Dept. of Engineering Science, University of Oxford, UK (2014-2015). Since 2015, he has been a Lecturer in the School of Computing, Electronics and Mathematics, Faculty of Engineering, Environment and Computing and an associate with the Research Institute Future Transport & Cities, Coventry University, UK. His research activities are in fault diagnosis, condition monitoring and degradation of electrical machines. He has authored/co-authored more than 60 papers in international scientific journals and conferences.